UDK/*UDC*: 556.166:624.074.1(078.9)
Izvirni znanstveni članek – *Original scientific paper*
DOI: 10.15292/acta.hydro.2025.03

Prejeto/*Received:* 06.02.2025
Sprejeto/*Accepted:* 24.04.2025
Objavljeno na spletu/*Published online:* 21.07.2025

3-D SIMULATIONS OF FLOW PAST A CYLINDRICAL BRIDGE PIER FOR DETERMINATION OF DRAG COEFFICIENT AS A FUNCTION OF FROUDE NUMBER

3D SIMULACIJE OBTEKANJA VALJASTEGA MOSTNEGA OPORNIKA ZA DOLOČITEV KOEFICIENTA UPORA V ODVISNOSTI OD FROUDOVEGA ŠTEVILA

Gorazd Novak [1], José Manuel Domínguez Alonso[2]

[1] Faculty of Civil and Geodetic Engineering, University of Ljubljana, Ljubljana, Slovenia
gorazd.novak@fgg.uni-lj.si
[2] EPhysLab, CIM-UVIGO, Universidade de Vigo, Ourense, Spain
jmdominguez@uvigo.es

Abstract

Increasingly frequent floods demonstrate the vulnerability of bridges and their piers. Designing a pier involves determining its drag coefficient C_d. In the existing literature, C_d is given as a function of the Reynolds number Re, i.e. $C_d = f(Re)$, while the present study also investigated C_d as a function of the Froude number Fr, i.e. $C_d = f(Fr)$. The SPH method and the model DualSPHysics were used to simulate three-dimensional turbulent free-surface flows past a surface-piercing cylinder in a straight horizontal channel. Subcritical, critical, and supercritical flows with $Fr < 2$ were examined. The model was calibrated for flows in a duct filled with water (i.e. flows without free water surface) and validated against open channel experiments from the literature. Finally, the model was used to simulate real-life high-discharge conditions. Determination of $C_d = f(Fr)$ indicated that the constant value of C_d as defined in the Eurocode 1 standard is not necessarily optimal.

Keywords: SPH, DualSPHysics, 3-D model, bridge pier, drag coefficient.

Izvleček

Vse pogostejše poplave izpostavljajo ranljivost mostov in mostnih opornikov. Pri dimenzioniranju mostnih opornikov je treba upoštevati njihov koeficient upora C_d. V večini virov je ta podan v odvisnosti od Reynoldsovega števila, tj. $C_d = f(Re)$, ta raziskava pa je obravnavala tudi C_d v odvisnosti od Froudovega števila. Z uporabo metode SPH in modela DualSPHysics so bile izvedene tridimenzionalne simulacije turbulentnega toka s prosto gladino, ki nastopa pri obtekanju valjastega mostnega opornika v ravnem horizontalnem kanalu. Širok razpon pretokov je zajel primere mirnega, kritičnega in deročega toka s

[1] Stik / *Correspondence*: gorazd.novak@fgg.uni-lj.si

Froudovimi števili $Fr < 2$. Model je bil umerjen na primere toka v pokritih kanalih brez proste gladine in nato validiran z eksperimenti na odprtem kanalu iz literature. Nazadnje je bil uporabljen za simulacije realističnih visokovodnih dogodkov. Določitev $C_d = f(Fr)$ je pokazala, da konstantna vrednost C_d, ki jo predpisuje standard Eurocode 1, ni nujno optimalna.

Ključne besede: SPH, DualSPHysics, 3D-model, mostni opornik, koeficient upora.

1. Introduction

The motivation for this study came from the alarming fact that recent floods in Slovenia damaged or destroyed more than 70 bridges (Administration of the Republic of Slovenia for Civil Protection and Disaster Relief, 2023). Designing of new bridges could include numerical models of bridge piers, like the one used in the present study. These simulations provided some interesting new insight into the relationship between drag coefficient C_d of a cylindrical object and Froude number Fr of the observed approach flow.

A bridge pier in a river is typically considered as a case of flow past a cylinder (e.g. Rajar, 1997; White, 2011), usually concerning the streamlines and the force of fluid acting on a solid object. This force results from the non-uniform distribution of fluid pressure and is taken into consideration in the design of piers. Although the flow conditions can be complex, including several kinds of vortices (Roulund et al., 2005), in most cases the following simplified expression is used to calculate the total drag force (Equation 1):

$$F_d = C_d \cdot \frac{\rho \cdot A \cdot u^2}{2} \quad (1),$$

where the drag force F_d is determined by the drag coefficient C_d, fluid density ρ, the object's cross-sectional area A (perpendicular to the direction of the flow), and flow velocity u (measured upstream of the disturbance caused by the object). C_d for circular cylinders is given as a function of the Reynolds number, $C_d = f(Re)$, decreasing from $C_d = 10$ for $Re = 1$ to $C_d = 1$ for $Re = 10^3$, followed by a significant decrease in C_d for Re between 10^5 and 10^6 due to the transition of the laminar boundary layer into a turbulent one (Rajar, 1997; White, 2011; Cengel & Cimbala, 2014). With the further increase of Re, the C_d gradually increases and becomes constant at approximately $C_d = 0.6$ (e.g. Rajar, 1997) or $C_d = 0.7$ (e.g. White, 2011) for $Re > 10^7$. It can be assumed that this was the basis for directions in the Eurocode standard EN 1991-1-6 (Eurocode, 2005), giving a very similar expression (Equation 2):

$$F_{wa} = \frac{1}{2} \cdot k \cdot \rho_{wa} \cdot h \cdot b \cdot v_{wa}^2 \quad (2)$$

Equation 2 includes the following: magnitude of the total horizontal force exerted by currents on the vertical surface F_{wa}, the mean speed of the water averaged over the depth v_{wa}, the water depth (not including local scour depth) h, the width of the object b, and the shape factor $k = 0.7$ for an object of circular horizontal cross-section (Eurocode 2005). The shape factor k in Eq. 2 is equivalent to the coefficient C_d in Eq. 1. By using the constant value $k = 0.7$, the standard remains on the safe side when dealing with more turbulent and therefore potentially more problematic real-life flows. However, it can be shown that using a constant C_d is not optimal. As mentioned, C_d is not constant within certain intervals of Re (see e.g. Rajar, 1997; White, 2011; Cengel & Cimbala, 2014), and this could indicate the need to use a non-constant expression for C_d.

Water flows around cylinders were investigated mostly concerning bridge pier scour (Roulund et al., 2005; Alabi, 2006; Huang et al., 2009; Akhlagi et al., 2020; Kim et al., 2022), debris jams (Panici & Almeida, 2018; Schalko et al., 2020; Zhang et al., 2023), and even in the design of fish passes elements (Cassan et al., 2014). Most investigations focusing on the effect of Reynolds and Froude numbers employ mostly numerical models (Koo et al., 2014), while experimental studies are less frequent. Chaplin & Teigen (2003) performed towing experiments, while Ducrocq et al. (2017) used a small physical model. 3-D numerical

approach remains less frequent and the present study addresses this gap.

The lack of experiments with larger hydraulic models could indicate that a bridge pier is typically regarded as a simple case of flow past a cylinder, where one only needs to read C_d from some sort of a $C_d = f(Re)$ table. However, such an approach could be too simplified because these tables were determined for flows in ducts filled with water without a free water surface, and for completely submerged objects. This might be sufficiently valid for most practical civil engineering cases with low flow velocities and almost horizontal water surfaces, but not when modelling a bridge pier resisting a high-discharge flood flow. During such events, the changes in water levels around a pier can be significant, resulting in a more non-uniform water pressure distribution and larger drag forces.

We suggest that, for real-life high discharges, the C_d values should be given as a function of the Froude number, i.e. $C_d = f(Fr)$, determined from experiments in larger physical and 3-D numerical models with a free water surface.

2. Method

This study used the smoothed particle hydrodynamics (SPH) method as employed in the DualSPHysics software. SPH is a Lagrangian meshless method that allows simulations of phenomena where Eulerian methods can be difficult to apply, e.g. violent free-surface flows. DualSPHysics is a weakly compressible SPH Navier–Stokes solver, as described in Domínguez et al. (2022). It is gaining in popularity due to its capability to simulate a variety of real-life engineering problems, e.g. turbine design (Hanousek et al., 2024), wave energy converters (Capasso et al., 2025), and even cardiovascular systems (Laha et al., 2025). In the present study, we built upon our previous work on flows past submerged objects (Novak et al., 2019) and flows over obstacles in fishways (Novak et al., 2021; Novak et al., 2023).

3. Results and discussion

3.1 Overview of simulations

The present research included three stages: 1) calibration, 2) validation, and 3) real-life application, as summarized in Table 1:

In each case, the inflow was equal to the outflow. This was achieved with boundary conditions that imposed inlet and outlet depths $h_{in} = h_{out}$ and velocities $u_{in} = u_{out}$. In the application stage, the simulated discharges ranged from $Q = B \cdot h_{in} \cdot u_{in} = 20 \cdot 1 \cdot 1 = 20 = \text{m}^3/\text{s}$ to as much as $25 \cdot 7 \cdot 5 = 875$ m^3/s.

Each stage was performed with a different numerical domain. To use the reference C_d values from the literature, which are given as $C_d = f(Re)$ for flows without a free water surface, the calibration was performed with a model of a duct filled with water (having no free water surface). The settings from the calibrated model were then used in the validation stage, where physical hydraulic model experiments were reproduced numerically. Finally, the calibrated and validated model was used in the real-life application stage, where $C_d = f(Fr)$ were determined for simulations of high-discharge events. A plan view of the domain used in the application stage and corresponding typical flow conditions are shown in Figure 1.

In all the cases, the channel was straight, with the cylinder placed on the channel's longitudinal axis. In most cases, the bed was horizontal, except for a few validation cases where a 1% slope was investigated as well. Simulations covered 20 s of physical time. Outputs were written for every 0.05 s of the physical time.

Water surface profiles were obtained with the DualSPHysics tool called MeasureTool, which calculated the depth of the fluid z over the location (x,y) from the corresponding column of fluid particles. Typical longitudinal sections of the model's water surface and the pier's outline are shown in Figure 2.

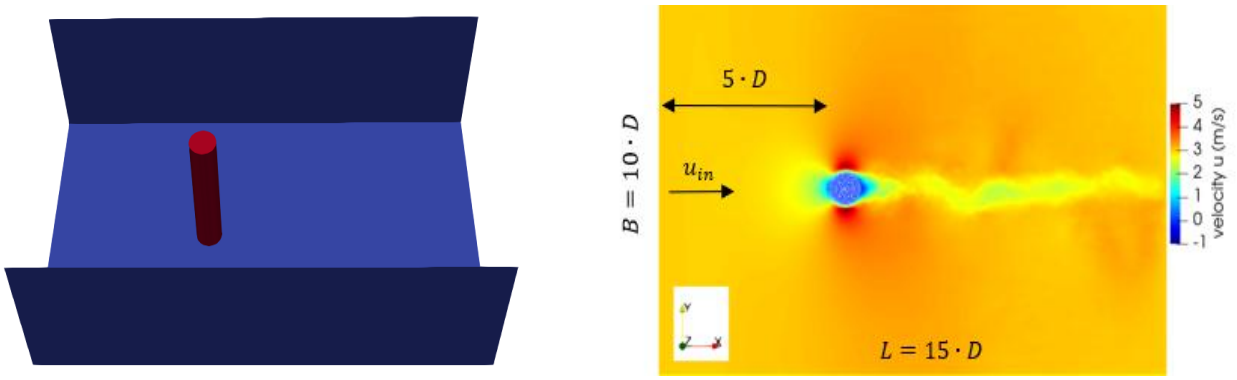

***Figure 1**: 3-D side view of the domain (left), and plan view of longitudinal velocity u at mid-depth ($z = 2.5$ m) of an open channel with a cylinder diameter $D = 2$ m, inlet depth $h_{in} = 5$ m, and inlet velocity $u_{in} = 3$ m/s.*

***Slika 1**: Prostorski prikaz domene (levo) in tloris vzdolžnih hitrosti $\boldsymbol{u}$ na srednji globini ($\boldsymbol{z = 2}$ m) odprtega kanala; premer valja je $\boldsymbol{D = 2}$ m, globina dotoka $\boldsymbol{h_{in} = 5}$ m, hitrost dotoka $\boldsymbol{u_{in} = 3}$ m/s.*

***Table 1**: Overview of test cases.*

***Preglednica 1**: Pregled obravnavanih primerov.*

stage	type of channel	pier diameter D [m]	channel width B [m]	channel length L [m]	inlet depth h_{in} [m]	inlet velocity u_{in} [m/s]	number of cases
1) calibration	duct	2	10 D	15 D	3	0.5 – 5	45
2) validation	open	0.04	10 D	100 D	0.04 – 0.10	0.31 – 0.63	8
3) application	open	2, 2.5	10 D	15 D	1, 2, 3, 5, 7	1 – 5	40

As expected, the water surface profiles remained almost horizontal for lower inlet velocities u. The water surface profile close to the pier changed with a higher inlet velocity. A higher u caused a water surface increase upstream of the pier, with a corresponding decrease downstream of the pier.

Inlet depth h_{in} was used to calculate the Froude number.

Forces of water acting on the pier were calculated with the DualSPHysics tool ComputeForces, which determined forces from the integration of fluid particles' accelerations. To calculate C_d, the longitudinal component F_x was used, calculated as an average of the last 5 seconds of the simulation.

In all simulations, a single GPU (NVIDIA GTX 1080) was used. Simulation runtime for a typical case with 2.2 million particles and 20 s of physical time amounted to 2.9 hours.

3.2 Calibration

The model was calibrated for cases of a rectangular duct filled with water that had a depth equal to the inlet height. The pier extended from the bottom to the top of the duct. Despite using a 3-D domain, the flow during the calibration was 2-D to reproduce the conditions for which the values $C_d = f(Re)$ are given in the literature.

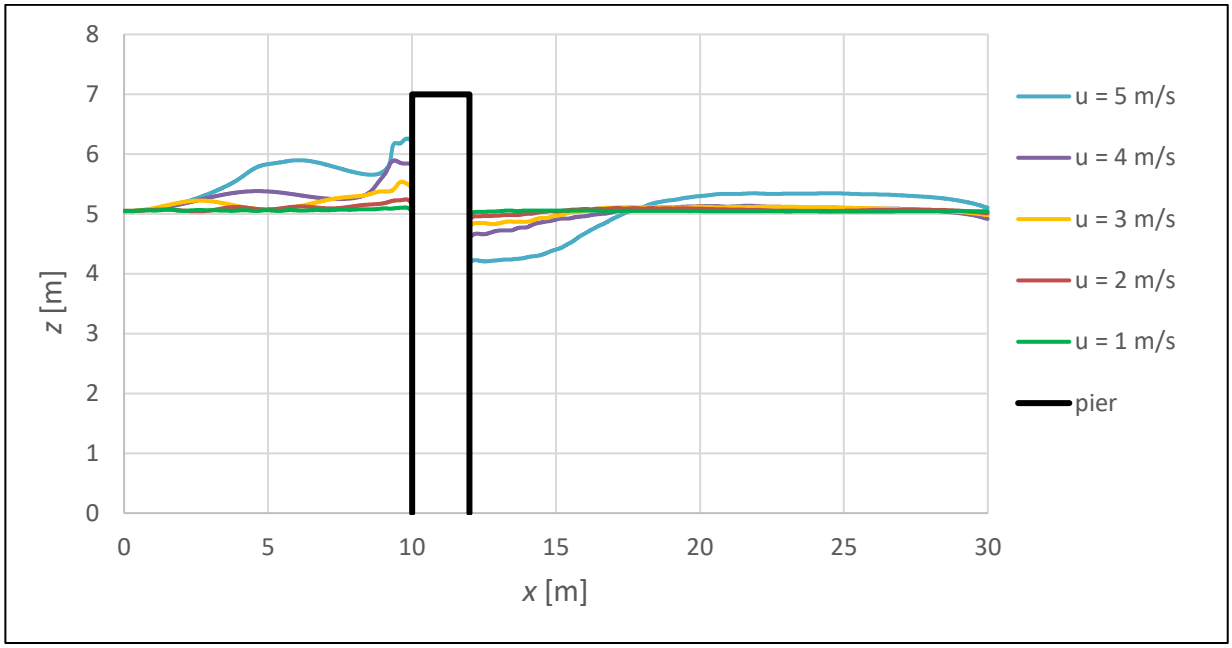

Figure 2: *Longitudinal water surface profile along the channel axis for cases with 5 m deep inflow.*

Slika 2: *Vzdolžni prerez gladine po osi kanala za primere z globino dotoka 5 m.*

The calibration focused on parameters that affect the model's accuracy. By changing the model's settings, the effect of the following main parameters was tested:

a) non-dimensional channel size, defined by width and length, expressed as B/D and L/D

b) viscosity, expressed as artificial viscosity α, or laminar (kinematic) viscosity in combination with the SPS turbulence model

c) ratio between the pier's diameter D and the initial interparticular distance dp, expressed as D/dp

d) smoothing length h, given non-dimensionally as h/dp. Note that smoothing length h is not related to inlet depth h_{in}.

The effect of these parameters was evaluated in terms of the resulting $C_d = f(Re)$. Rather than adjusting a single parameter, a combination of these settings needs to be right to get optimal results (i.e. those closest to the reference values from the literature), but details on such a parametric study are beyond the scope of this paper. More details about the parameters of SPH simulations can be found in Domínguez et al. (2022).

The calibration process proved the following settings as optimal: channel dimensions $B = 10D$ by $L = 15D$, kinematic viscosity $\nu = 10^{-6}$ m²/s with SPS turbulence model, resolution ratios $D/dp = 20$ and $h/dp = 1.8$. Using these settings, the calculated drag coefficients were close to the values from the literature (e.g. Rajar, 1997), as shown in Figure 3. Note that, as a result of the calibration, the C_d was calculated in relation to Re, in contrast to $C_d = f(Fr)$ of the validation and application stages, as explained in the following sections.

Figure 3 shows that for lower Re (with $u = 0.5$ and $u = 1$ m/s) the calculated C_d differed from the reference, but with increasing Re (i.e. larger u), the accordance improved. Comparison of $C_{d,model}$ against $C_{d,ref}$ for $Re \geq 2 \cdot 10^6$ gave a linear relation with correlation $R^2 = 0.88$. As mentioned, the following validation and application stages employed the simulation parameters that were optimised during the calibration stage.

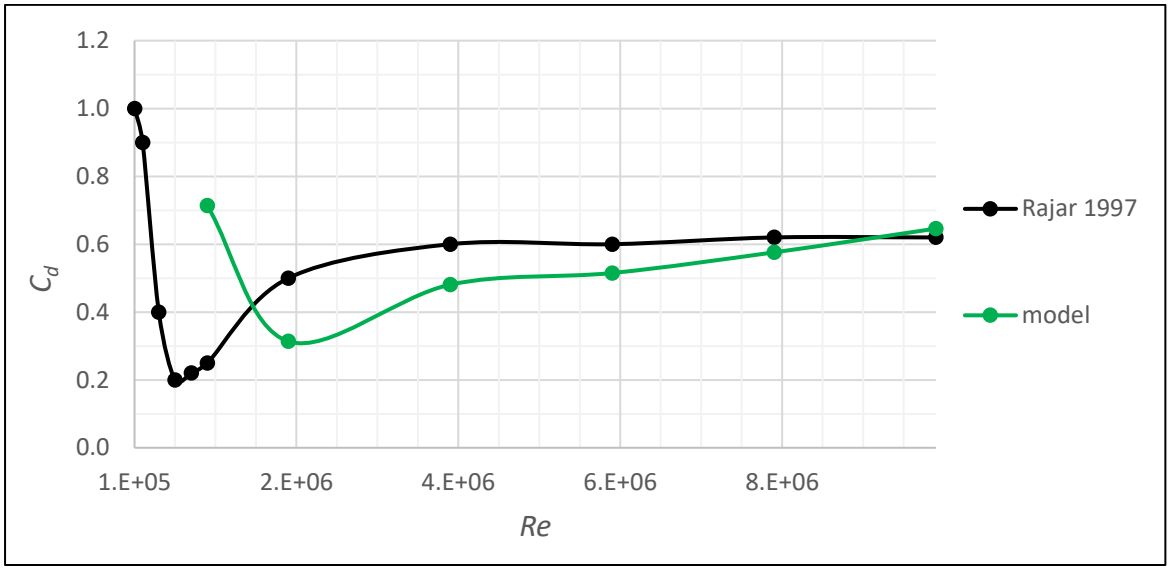

Figure 3: *Results of calibration for cases of a covered channel,* $\boldsymbol{h_{in} = 3}$ *m.*

Slika 3: *Rezultati umerjanja za primere pokritega kanala,* $\boldsymbol{h_{in} = 3}$ *m.*

3.3 Validation

Due to a lack of experimental data from larger physical models, the validation stage was based on the results obtained in a small physical model of an open channel by Ducrocq et al. (2017). A similar approach was made by Majtan et al. (2021) using SPH, but for other goals. Ducrocq et al. (2017) used a physical model of 4 m by 0.4 m to observe flows up to 25 l/s, with Re around 50000 and $Fr < 2.5$ (all but 4 of their experimental points were within $Fr < 2$). To avoid any additional uncertainty, our validation was limited to the numerical reproduction of experiments where the channel bed slope was 0 or 1% and there was no effect of the tailwater, while in some of their cases, Ducrocq et al. (2017) used a downstream sill as well. The results of the validation are shown in Figure 4.

Figure 4 shows that the results of both experiment and simulation were scattered in two distinctive groups. For subcritical flows ($Fr < 1$), the experimental values of C_d increased with Fr, ranging from 0.78 to 2.0, while the corresponding simulation results were between 1.03 to 1.89, meaning the difference between the experiment and the simulation was 32% in the lower range and 6% in the higher range. For supercritical flows ($Fr > 1$), the experimental values of C_d were lower, ranging from 0.55 to 1.63, and with increasing Fr they slowly decreased towards the value of around 0.6. Corresponding simulation results were within the area of scattered experimental points; values of C_d were between 1.02 and 1.33. Simulations results did not reach above $Fr = 1.5$ due to the limited choice of available validation cases.

3.4 Simulations of high-discharge conditions

In the final stage, the calibrated and validated model was used to simulate high-discharge conditions, as these are the most interesting for civil engineering applications. Real-life dimensions were taken into consideration with pier diameter measuring up to $D = 2.5$ m and flow depth ranging up to $h_{in} = 7$ m. The results of this stage were $C_d = f(Fr)$ as shown in Figure 5. To allow comparison, results from the validation stage were included in the figure as well, denoted as D = 0.04. Also shown in Figure 5 is a constant value of $C_d = 0.7$, proposed as shape factor k in the aforementioned standard. Note that, in the standard, the k is not given in relation to Fr, as Fr is not mentioned there.

Figure 5 confirms trends from the experiments: in the subcritical region, C_d values increased with Fr, close to the critical region where they achieved their maximum (value 1.8, experiment up to 2.0), while

they decreased with increasing Fr in the supercritical region.

The standard's constant value of $C_d = 0.7$ is not close to the results of the experiment or the simulation, especially in the region $Fr = 0.8 - 1.3$. Note that all the points from Figure 5 combined cover a wide range of discharges and that the standard value is different for the majority of these cases. Due to the impact of C_d on the design of actual bridge piers, the issue warrants further attention, preferably supported with larger physical model experiments.

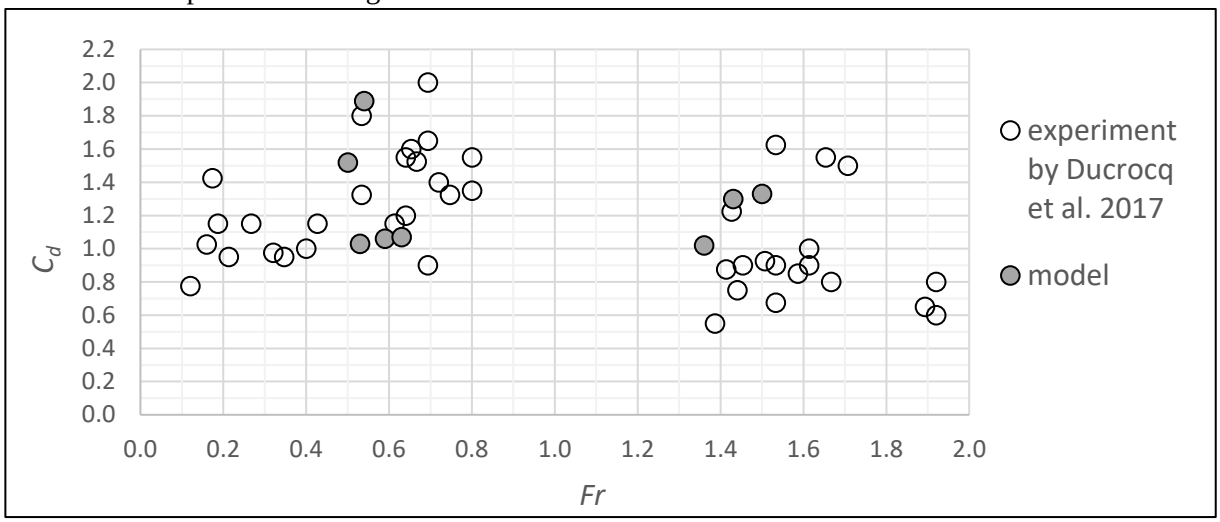

Figure 4: *Results of verification against experimental data by Ducrocq et al. (2017).*

Slika 4: *Rezultati verifikacije z eksperimentalnimi rezultati študije Ducrocq et al. (2017).*

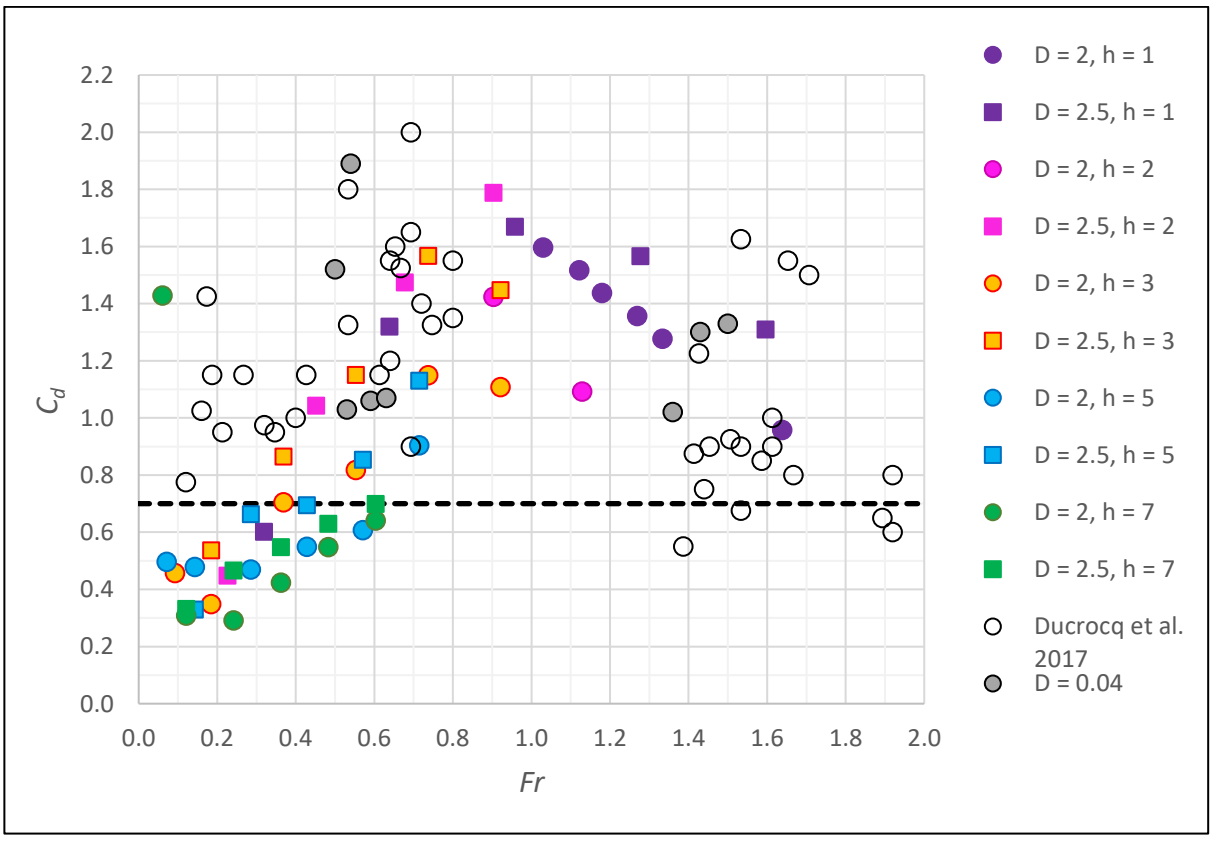

Figure 5: *Results of the application stage: drag coefficient as a function of Froude number.*

Slika 5: *Rezultati aplikativne faze: koeficient upora v odvisnosti od Froudovega števila.*

4. Conclusions

The presented results confirmed our initial hypothesis that, for real-life high-discharge events, the values of C_d should not be regarded as a constant, as prescribed in the Eurocode 1 standard, but as a function of Froude number, i.e. $C_d = f(Fr)$, and determined with models of free-surface water flows.

A 3-D numerical model based on the SPH method was used to calculate drag coefficient values for a wide range of flows, including cases of a fully submerged cylinder in a duct (without free water surface) and cases of surface-piercing cylinders in an open channel.

Calibrated against reference values $C_d = f(Re)$ from the literature and validated against the experimental results of a physical hydraulic model, the numerical model was used to calculate $C_d = f(Fr)$ for cases resembling real-life high-discharge conditions. Both experiments and simulations indicated that $C_d = f(Fr)$ increased with Fr in the subcritical region and decreased in the supercritical one. Thus, it can be concluded that the premise of the Eurocode standard EN 1991-1-6 is insufficient where it suggests that one should use the constant value of the drag coefficient (or shape factor) at 0.7 regardless of the flow regime. Note that this insufficiency affects the computation of the drag force and thus the design of a bridge pier.

An improved formulation of non-constant $C_d = f(Fr)$ for real-life civil engineering applications would require larger physical model experiments to provide additional calibration and validation data for 3-D numerical models.

CRediT authorship contribution statement:

Conceptualization: GN, JMDA. Data curation: GN, JMDA. Formal analysis: GN, JMDA. Investigation: GN. Methodology: JMDA, GN. Software: JMDA. Validation: GN. Visualization: GN, JMDA. Writing – original draft: GN. Writing – review & editing: GN, JMDA.

Data availability

Article is based on the results of simulations.

Declaration of interest

The authors declare no conflicts of interests. No AI methods have been used in paper writing or paper preparation.

Funding

GN acknowledges funding by the Slovenian Research and Innovation Agency (ARIS): P2-0180. JMDA acknowledges funding from the grant CNS2022-136073 funded by MCIN/AEI/ 10.13039/501100011033 and by "European Union NextGenerationEU/PRTR" and the grant RYC2022-038341-I funded by MCIN/AEI/10.13039/501100011033 and by "ESF Investing in your future". This work was also partially financed by the project ED431C 2021/44 “Programa de Consolidación e Estruturación de Unidades de Investigación Competitivas” financed by Xunta de Galicia, Consellería de Cultura, Educación e Universidade.

References

Akhlaghi, E., Babarsad, M.S., Derikvand, E., Abedini, M. (2020). Assessment the Effects of Different Parameters to Rate Scour around Single Piers and Pile Groups: A Review. *Archives of Computational Methods in Engineering* **27**, 183 – 197. https://doi.org/10.1007/s11831-018-09304-w.

Alabi, P.D. (2006). Time development of local scour at a bridge pier fitted with a collar, Master Thesis, University of Saskatchewan, 211 p.

Administration of the Republic of Slovenia for Civil Protection and Disaster Relief (2023). Floods in Slovenia, August 2023 - Presentation at CROSScade Workshop – Lessons learned from recent flood events in Slovenia & Croatia, Ljubljana, 27.10.2023

Capasso, S., Tagliafierro, B., Martínez-Estévez, I., Altomare, C., Gómez-Gesteira, M., Göteman, M., Viccione, G. (2025). Development of an SPH-based numerical wave-current tank and application to wave energy converters. *Applied Energy* **377B**, 124508. https://doi:10.1016/j.apenergy.2024.124508.

Cassan, L., Tien, T.D., Courret, D., Laurens, P., Dartus, D. (2014). Hydraulic Resistance of Emergent Macroroughness at Large Froude Numbers: Design of Nature-Like Fishpasses. *Journal of Hydraulic Engineering* **140(9)**, 04014043.

https://doi.org/10.1061/(ASCE)HY.1943-7900.0000910.

Cengel, Y.A., Cimbala, J.M. (2014). Fluid Mechanics – Fundamentals and Applications. Third edition. McGraw-Hill, New York, 1000 p.

Chaplin, J.R.,Teigen, P. (2003). Steady flow past a vertical surface-piercing circular cylinder. *Journal of Fluids and Structures* **18**, 271 – 285. https://doi.org/10.1016/j.jfluidstructs.2003.07.009.

Domínguez, J.M., Fourtakas, G., Altomare, C., Canelas, R.B., Tafuni, A., García-Feal, O., Martínez-Estévez, I., Mokos, A., Vacondio, R., Crespo, A.J.C., Rogers, B.D., Stansby, P.K., Gómez-Gesteira, M. (2022). DualSPHysics: from fluid dynamics to multiphysics problems. *Computational Particle Mechanics* **9**, 867 – 895. https://doi.org/10.1007/s40571-021-00404-2.

DualSPHysics (2025). Available at: https://dual.sphysics.org/ (accessed 4.2.2025).

Ducrocq, T., Cassan, L., Chorda, J., Roux, H. (2017). Flow and drag force around a free surface piercing cylinder for environmental applications. *Environmental Fluid Mechanics* **17**, 629 – 645. https://doi.org/10.1007/s10652-016-9505-9.

Hanousek, N., Ranabhat, B., English, A., Ahmadian, R. (2024). A Smoothed Particle Hydrodynamics method for vertical axis turbine design and assessment. *Journal of Hydrodynamics*, **36**, 991 – 1007. https://doi:10.1007/s42241-024-0074-y.

Huang, W., Yang, Q., Xiao, H. (2009). CFD modeling of scale effects on turbulence flow and scour around bridge piers. *Computers & Fluids* **38**, 1050 – 1058. https://doi.org/10.1016/j.compfluid.2008.01.029.

Kim, H.S., Chen, H.-C., Briaud, J.-L. (2022). Numerical Simulation of Scour Hole Backfilling in Unidirectional Flow. *Journal of Hydraulic Engineering* **148(7)**, 04022013 https://doi.org/10.1061/(ASCE)HY.1943-7900.0001982.

Koo, B., Yang, J., Yeon S.M., Stern, F. (2014). Reynolds and Froude number effect on the flow past an interface-piercing circular cylinder. *International Journal of Naval Architecture and Ocean Engineering* **6**, 529 – 561. https://doi.org/10.2478/IJNAOE-2013-0197.

Laha, S., Fourtakas, G., Das, P.K., Keshmiri, A. (2025). Graphics processing unit accelerated modeling of thrombus formation in cardiovascular systems using smoothed particle hydrodynamics. *Physics of Fluids*, **37(2)**, 021902. https://doi:10.1063/5.0250640.

Majtan, E., Cunningham, L.S., Rogers, B.D. (2021). Flood-Induced Hydrodynamic and Debris Impact Forces on Single-Span Masonry Arch Bridge. *Journal of Hydraulic Engineering* **147(11)**, 04021043. https://doi.org/10.1061/(ASCE)HY.1943-7900.0001932.

Novak, G., Domínguez, J.M., Tafuni, A., Četina, M., Žagar, D. (2019). Določitev koeficienta upora potopljenega telesa z uporabo metode SPH (Evaluation of the drag coefficient of a fully submerged body using SPH). *Acta hydrotechnica* **32/57** (in Slovenian) https://doi.org/10.15292/acta.hydro.2019.08.

Novak, G., Domínguez, J.M., Tafuni, A., Silva, A.T., Pengal, P., Četina, M., Žagar, D. (2021). *Water* **13**, 1595. https://doi.org/10.3390/w13111595.

Novak, G., Pengal, P., Silva, A.T., Domínguez, J.M., Tafuni, A., Četina, M., Žagar, D. (2023). Interdisciplinary design of a fish ramp using migration routes analysis. *Ecological Modelling* **475**, 110189. https://doi.org/10.1016/j.ecolmodel.2022.110189.

Rajar, R. (1997). Hidromehanika. Univerza v Ljubljani, Fakulteta za gradbeništvo in geodezijo, Ljubljana, 235 p. (in Slovenian).

Panici, D., de Almeida, G.A.M. (2018). Formation, growth, and failure of debris jams at bridge piers. *Water Resources Research* **54**, 6226 – 6241. https://doi.org/10.1029/2017WR022177.

Roulund, A., Sumer B.M., Fredsøe J., Michelsen J. (2005). Numerical and experimental investigation of flow and scour around a circular pile. *Journal of Fluid Mechanics* **534**, 351 – 401 https://doi.org/10.1017/S0022112005004507.

Schalko, I., Schmocker, L., Weitbrecht, V., Boes, R.M. (2020). Laboratory study on wood accumulation probability at bridge piers. *Journal of Hydraulic Research* **58(4)**, 566 – 581. https://doi.org/10.1080/00221686.2019.1625820.

Standard EN 1991-1-6:2005 Eurocode 1: Actions on structures – Part 1-6: general actions – Actions during execution

White, F.M. (2011). Fluid Mechanics – Seventh Edition, McGraw-Hill, New York, 885 p.

Zhang, W., Rennie, C.D., Nistor, I. (2023). Experimental investigation of the hydrodynamic field around a half-cone woody debris jam on a bridge pier. *Journal of Hydraulic Research* **61(6)**, 866– 879. https://doi.org/10.1080/00221686.2023.2259859.